


A Statistical Approach to Violin Evaluation

Raffaele Malvermi ^{1,*} , Sebastian Gonzalez ¹, Fabio Antonacci ¹, Augusto Sarti ¹ and Roberto Corradi ²

¹ Department of Electronics, Information and Bioengineering, Politecnico di Milano, 20133 Milano, Italy; tsuresuregusa@gmail.com (S.G.); fabio.antonacci@polimi.it (F.A.); augusto.sarti@polimi.it (A.S.)

² Department of Mechanical Engineering, Politecnico di Milano, 20156 Milano, Italy; roberto.corradi@polimi.it

* Correspondence: raffaele.malvermi@polimi.it

Featured Application: Physics-informed quality assessment of a stringed musical instrument.

Abstract: Comparing violins requires competence and involves both subjective and objective evaluations. In this manuscript, vibration tests were performed on a set of 25 violins, both historical and new. The resulting bridge admittances were modeled in the low and mid-frequency ranges through a set of objective features. Once projected into the new representation, the bridge admittances of three historical violins made by Stradivari and a famous reproduction revealed high similarity. PCA highlighted the importance of signature mode frequencies, bridge hill behavior, and signature mode amplitudes in distinguishing different violins.

Keywords: musical acoustics; bridge admittance; feature-based



Citation: Malvermi, R.; Gonzalez, S.; Antonacci, F.; Sarti, A.; Corradi, R. A Statistical Approach to Violin Evaluation. *Appl. Sci.* **2022**, *12*, 7313. <https://doi.org/10.3390/app12147313>

Academic Editors: Mariana Domnica Stanciu, Voichița Bucur and Mircea Mihălcică

Received: 26 June 2022

Accepted: 19 July 2022

Published: 21 July 2022

Publisher's Note: MDPI stays neutral with regard to jurisdictional claims in published maps and institutional affiliations.



Copyright: © 2022 by the authors. Licensee MDPI, Basel, Switzerland. This article is an open access article distributed under the terms and conditions of the Creative Commons Attribution (CC BY) license (<https://creativecommons.org/licenses/by/4.0/>).

1. Introduction

Assessing the quality of a violin is an extremely difficult matter. There are no objective descriptors that can separate a “good” violin from a “great” one and yet some instruments can reach prices up in the millions. Even professional musicians have trouble distinguishing old from new violins, and their preference does not necessarily correlate with the price of the instrument [1–3]. At the end of the day, it comes down to the subjective preference of the player. Having an objective measure to support the evaluation of an instrument could help instrument makers and musicians in the search for the perfect match between violinist and violin.

The bridge admittance could be such a simple objective tool to qualify an instrument. This is the frequency response function (FRF) measured at the bridge on the plane perpendicular to the strings. The measurement is performed by means of an instrumented hammer and an accelerometer, located at opposites on the bridge. It is a good estimator of the vibrational behavior of the instrument soundbox from whence the sound of the violin comes from. It is fast to perform and the equipment needed is relatively cheap, at least for a scientific lab if not for the luthier’s workshop [4,5].

FRFs have in fact been used for a long time as descriptors of the violin in the literature [6,7]. It has even been stated, without hard evidence though, that the quality of the violin correlates with some spectral features of the bridge admittance. In particular, the presence of the so-called bridge hill has been hailed as a mark of quality. According to [7], this bridge hill is “a hump [sic] between 2 and 3 kHz in their frequency responses”. Despite the importance of this feature, the lack of a scientifically grounded definition makes its use in research questionable.

Our objective in this article is to produce physically informed and objectively measurable features from the bridge admittance that allow one to compare, and maybe eventually discriminate, good violins from great ones. At the very least, have a standard way of comparing them beyond the mere visual inspection, which seems to be the preferred way in the state of the art [5].

To compare different FRFs one needs to understand their physical provenance. Woodhouse [8] divides the signal into three separate regions. In the low range, the influence of the individual modes of the instrument is clearly visible in the signal as peaks. Eventually, as the frequency of the modes becomes higher, the damping factor makes the peaks blend together and a clear identification of the modes is not possible: these are the transitional modes. At high frequency, in fact, the mode overlap becomes greater, and even small differences cause a great variability of the mode shapes between instruments. Although the modes still determine the behavior of the FRF, analytical approaches to model it becomes progressively less effective [9].

Different instruments have different resonance frequencies. These differences are due to material and geometric variation between the instruments [10]. Therefore, a direct comparison in the frequency domain is not immediately applicable. If two instruments have the same FRFs but shifted in a few Hertz, does that make them more similar than a pair of FRFs where the modes are at the same frequency but their amplitude is completely different? Developing a way to answer those kinds of questions is the aim of this article.

Following the separation highlighted by Woodhouse, one can consider different models for each frequency range of the FRF. Modal approaches are revealed as powerful reconstructions of the individual (also denoted as “signature”) and transitional modes. Indeed, the bridge can be interpreted as a filter coupling strings and violin soundbox such that its admittance can be seen as the filter transfer function [11]. Accordingly, the fundamental properties of modes, i.e., frequency, amplitude, and damping ratio, can be used to define the poles and zeros of such filter. From the signal processing perspective, this methodology can be applied not only in the analysis stage [12] but also in the synthesis of virtual or altered instrument timbre starting from measured admittances [13–15].

Although they can fit a large portion inside acoustic instrument admittances, these models are not able to interpret relevant high-frequency components. At the same time, they could need a large number of modes to reach good accuracy [13]. The same considerations hold for Euclidean distances computed even on a small set of signature mode features. These showed to better quantify the similarity between FRFs if compared to point measures, e.g., mean square error (MSE), which are evaluated in the frequency domain directly [16]. However, the same metric fails when differences occur mainly at high frequency.

In this work, we propose an extension of the multidimensional feature space proposed in [16] based on both modal parameters and energy-based descriptors, found to be more representative for the mid-range [9]. In this new representation, a more informative Euclidean distance can be measured to assess the similarity between FRFs in the low and mid-frequency ranges. The features adopted here are objectively defined, in contrast to e.g., the bridge hill, and could be used to study the perceptual relevance of particular elements of the FRF through virtual sound synthesis.

2. Materials and Methods

2.1. Violins

The selection of violins under study counts twenty-five instruments with varying ages and styles of making. Thirteen of these belong to the permanent collection of instruments awarded in the “Antonio Stradivari International Triennial Competitions of Stringed instrument making” [17]. The competition, held in the city of Cremona since 1976, embraces both Cremonese and international competitors. A jury of experts selects the winner according to stylistic and technical evaluations. The winner of each contest is acquired by the museum and kept in its permanent collection. Among the remaining samples, there are nine modern violins that were kindly offered by violin makers during the Mondo Musica 2020 exposition and three historical violins made by Stradivari in the 18th century. For all the instruments, the owners provided consent for the usage of the results in an anonymous fashion. For this reason, and for the ease of reading, we will denote all the violins made within the 20th and 21st centuries with M1–M22 (modern) while we will refer to the historical ones as H1–H3. It is noteworthy that one of the modern violins (i.e., M22) was made by a famous

international violin maker with the aim of reproducing the outline of one of the measured historical violins (i.e., H3). The acoustic similarity of the violins was confirmed by the actual owner of both instruments, who happens to be an internationally acclaimed violin player. Although dissimilarities between violins rely often on subtle details and even two replicas of the same violin could easily differ in their sound [3], the presence of the pair M22–H3 in addition to a group of violins belonging to the same author, i.e., to Stradivari, still could be used to assess the soundness of the proposed metric. Indeed, common trends are expected to be observed once the bridge admittances are projected into the feature representation.

2.2. Vibration Tests

The bridge admittances were measured by means of hammer impact testing. A structure made of wood and rubber bands was built to approximate free boundary conditions during the test. Four rubber bands were used for the suspension of the instrument, letting the sample hang in a vertical position and minimizing the contact surface [18,19]. In particular, two rubber bands were placed at the bottom of the violin while the remaining two supported its soundbox from the upper corners. In this configuration, the resting position of the hammer is vertical after the hit, avoiding the occurrence of accidental secondary strikes during the acquisition. A dynamometric hammer with light tip (086E80, by PCB Piezotronics) and a uniaxial accelerometer (352A12, by PCB Piezotronics) were used to generate an impulsive excitation and measure the harmonic response, respectively. Impacts were applied on one edge of the bridge while the accelerometer was placed on the opposite side. For each measurement, six time-domain signals of two seconds sampled at 48 kHz were acquired. FRFs were then estimated following the definition of the H1 estimator to reduce noise caused by the instrumentation [20]. The magnitudes of the resulting FRFs are represented in dB scale, with a reference value equal to $1 \text{ m s}^{-1} \text{ N}^{-1}$.

2.3. Low-Frequency Features

The signature modes of a violin typically cover the violin response in the low-frequency range, which can reach 800 Hz for the complete soundbox [21]. Thanks to the low modal density encountered in this region, analytical approximations based on modal superposition can be used [22]. Therefore, let us model a given bridge admittance $H_{ij}(\omega)$ as a linear combination of modal contributions, namely

$$H_{ij}(\omega) \sim \sum_{r=1}^N \frac{\Phi_{ri}\Phi_{rj}}{\omega_r^2 + 2j\omega\zeta_r\omega_r - \omega^2}, \quad \omega \in [\omega_{min}, \omega_{mid}], \quad (1)$$

where i and j refer to the excitation and measurement points at the bridge corners, N is the number of signature modes considered, Φ_{ri} and Φ_{rj} correspond to the mode shape of mode r evaluated at the two points observed, ω_r is the natural frequency and ζ_r is the damping ratio associated to mode r , respectively.

The model was defined using as features the frequency $f_r = \omega_r/2\pi$, amplitude $p_r = |H_{ij}(\omega_r)|$ and Q factor $q_r = 1/2\zeta_r$ of $N = 4$ signature modes among the ones presented in the literature [21], namely: (i) the Helmholtz mode A0 (features f_1, p_1, q_1); (ii) the C Bouts Rhomboidal mode CBR (f_2, p_2, q_2); (iii) the Corpus mode B1– (f_3, p_3, q_3); (iv) the Body mode B1+ (f_4, p_4, q_4). The choice was made on the basis of two main considerations. On the one hand, the selected modes proved to be consistent over frequency throughout the set of bridge admittances analyzed while mode switching occurred frequently for the excluded ones. As an example, the second air mode A1 was found either between CBR and B1– or between B1– and B1+, making its identification impossible for a simple peak finding algorithm. On the other hand, these modes are also well-known by the violin maker community [8,23].

The frequency range in which the reconstruction shows a good agreement with the measurement has $\omega_{min} = 2\pi f_{min}$ with $f_{min} = 230$ Hz as lower limit to exclude irrelevant information before the A0 mode and, as upper limit, $\omega_{mid} = 2\pi f_{mid}$ with f_{mid} equal to the

frequency of the first antiresonance (i.e., minimum in the FRF magnitude) after the B1+ mode. This antiresonance was taken as a reference since it was found in all the FRFs under study. It is worth noticing that when ω matches ω_r ,

$$|H_{ij}(\omega_r)| \sim \frac{\Phi_{ri}\Phi_{rj}}{2\xi_r\omega_r^2}, \tag{2}$$

thus making Equation (1) completely recovered from the knowledge of the mode frequencies, amplitudes and corresponding damping ratios.

Finally, a total of twelve low-frequency descriptors are included in the definition of the feature space. We will denote the features related to signature mode frequencies as the vector $\mathbf{f} = [f_1, f_2, f_3, f_4]$, the features related to signature mode amplitudes as the vector $\mathbf{p} = [p_1, p_2, p_3, p_4]$ and the features related to damping as the vector of corresponding Q factors $\mathbf{q} = [q_1, q_2, q_3, q_4]$. If \mathbf{f} is extracted directly from the measured signal by means of available peak finding algorithms, \mathbf{p} and \mathbf{q} must be tuned such that the model takes into account the correlation between modes, even though this was found to be low. The estimates for these two subsets of features are thus obtained rewriting Equation (1) as a function of \mathbf{p} and \mathbf{q} and setting up a least-square measurement fitting problem as

$$\min_{\mathbf{p}, \mathbf{q} \in \mathbb{R}^+} \left\| |H_{ij}(\omega)| - \left| \sum_{r=1}^4 \frac{\omega_r^2 p_r}{q_r(\omega_r^2 - \omega^2) + j\omega\omega_r} \right| \right\|_2^2, \tag{3}$$

with $\omega \in [\omega_{min}, \omega_{mid}]$ and $\omega_r = 2\pi f_r$. The minimization was solved iteratively using the simplex algorithm. The peak amplitudes extracted from the signal were provided as initial values for \mathbf{p} while a guess for \mathbf{q} was computed by means of the half-power bandwidth method [24].

2.4. Mid-Frequency Features

To define a set of features modeling the FRF at higher frequencies, we took inspiration from statistical approaches to the subject [9]. We chose to represent the energy distribution of a given bridge admittance $H_{ij}(\omega)$ by computing its relative power (RP) as

$$RP(\omega) = \frac{P(\omega)}{P_{tot}} = \frac{\int_{\omega_{min}}^{\omega} |H_{ij}(\omega)|^2 d\omega}{\int_{\omega_{min}}^{\omega_{max}} |H_{ij}(\omega)|^2 d\omega}, \tag{4}$$

where $P(\omega)$ is the cumulative power and P_{tot} is the total power of the signal, i.e., computed within the range $[2\pi f_{min}, 2\pi f_{max}]$ with $f_{min} = 230$ Hz and $f_{max} = 4500$ Hz. In the frequency interval considered, $RP(\omega)$ ranges between 0 and 1.

The slope of this descriptor is characterized by “bumps” where the corresponding bridge admittance exhibits high-energy components (see Figure 1b as an example). In particular, two main slope changes typically occur in violin bridge admittances after 500–600 Hz and between 2 and 3 kHz. The first relevant increase in the RP value, encountered at low frequencies, quantifies the amount of energy of the signature modes. Indeed, the RP curve starts to flatten at the frequency of mode B1+. Starting from the antiresonance after mode B1+, the RP shows a different growth rate for each violin in the dataset. Here, the RP curve exhibits a characteristic S-shape strongly correlated to a high-energy region in the corresponding bridge admittance.

To obtain a compact description of this behavior in the mid-frequency range, being it the interval between ω_{mid} and ω_{max} , we modelled the RP curve by means of a sigmoid function with tunable curvature based on [25], namely

$$\sigma(\omega, \omega^*, k^*) = \frac{\tilde{\omega} - k^* \tilde{\omega}}{k^* - 2k^* |\tilde{\omega}| + 1} \quad \text{where} \quad \tilde{\omega} = \frac{\omega - \omega^*}{\Delta\omega}, \tag{5}$$

ω^* is the center frequency of the sigmoid, k^* the control parameter for its curvature and $\overline{\Delta\omega} = \min(|\omega^* - \omega_{mid}|, |\omega_{max} - \omega^*|)$ such that the domain of the sigmoid is symmetric with respect to ω^* . To better fit the RP values at the extremes of the mid-frequency range, the output of the function $\sigma(\omega, \omega^*, k^*)$ is scaled and shifted leading to

$$\begin{aligned} \sigma'(\omega, \omega_{mid}, \omega^*, k^*) &= \sigma(\omega, \omega^*, k^*) \frac{RP(\omega^* + \overline{\Delta\omega}) - RP_{mid}}{\bar{\sigma}_{max} - \bar{\sigma}_{min}} + |RP_{mid} - \bar{\sigma}_{min}|, \\ RP_{mid} &= RP(\omega_{mid}), \\ \bar{\sigma}_{max} &= \max(\sigma(\omega, \omega_{mid}, \omega^*, k^*)), \\ \bar{\sigma}_{min} &= \min(\sigma(\omega, \omega_{mid}, \omega^*, k^*)). \end{aligned} \quad (6)$$

The fitting was performed by searching for the values of ω^*, k^* such that the MSE between the measured RP and the predicted sigmoid has its minimum. The minimization was carried out iteratively using the simplex algorithm. Interestingly enough, the values found for k^* at the end of the optimization follow a Gaussian distribution centered around -0.7 . Two outliers were detected, with k^* equal to -0.25 and -0.05 .

The advantage of this representation is that the resulting optimal sigmoid model can be easily projected back to the frequency-magnitude space by computing its derivative with respect to ω . We thus decided to use the parameters of Equation (6) as features for the mid-frequency range.

Along with these features, we added two additional descriptors to the set. On the one hand, we took the MSE between the measured RP and the sigmoid fit as a metric of the fitting accuracy. We will denote it as the “area difference” ΔA for its geometric interpretation (see Figure 1b). On the other hand, we considered the slope k_{high} of the linear fit in the range [4000, 4500] Hz since the sigmoid model fails at explaining the linear decrease in the magnitude encountered in FRFs at very high frequency. Table 1 summarizes the final set of low and mid-frequency features defined to reconstruct a bridge admittance.

Table 1. Summary of the low and mid-frequency features defined.

Name	Description
Signature mode frequencies	
f_1	Frequency of the first signature mode (Helmoltz mode, A0)
f_2	Frequency of the second signature mode (C Bouts Rhomboidal mode, CBR)
f_3	Frequency of the third signature mode (Corpus mode, B1−)
f_4	Frequency of the fourth signature mode (Body mode, B1+)
Signature mode amplitudes	
p_1	Amplitude of the first signature mode (Helmoltz mode, A0)
p_2	Amplitude of the second signature mode (C Bouts Rhomboidal mode, CBR)
p_3	Amplitude of the third signature mode (Corpus mode, B1−)
p_4	Amplitude of the fourth signature mode (Body mode, B1+)
Signature mode damping	
q_1	Q Factor of the first signature mode (Helmoltz mode, A0)
q_2	Q Factor of the second signature mode (C Bouts Rhomboidal mode, CBR)
q_3	Q Factor of the third signature mode (Corpus mode, B1−)
q_4	Q Factor of the fourth signature mode (Body mode, B1+)

Table 1. Cont.

Name	Description
Mid-frequency	
ω_{mid}	Frequency of the first antiresonance after mode B1+
RP_{mid}	Relative power of the signature modes, $RP_{mid} = RP(\omega_{mid})$
ω^*	Sigmoid center frequency
RP^*	Relative power center value, $RP^* = RP(\omega^*)$
k^*	Relative power curvature
ΔA	Area difference, $\Delta A = MSE(RP(\omega), \sigma'(\omega, \omega_{mid}, \omega^*, k^*))$
k_{high}	Slope of the linear fit at high frequency

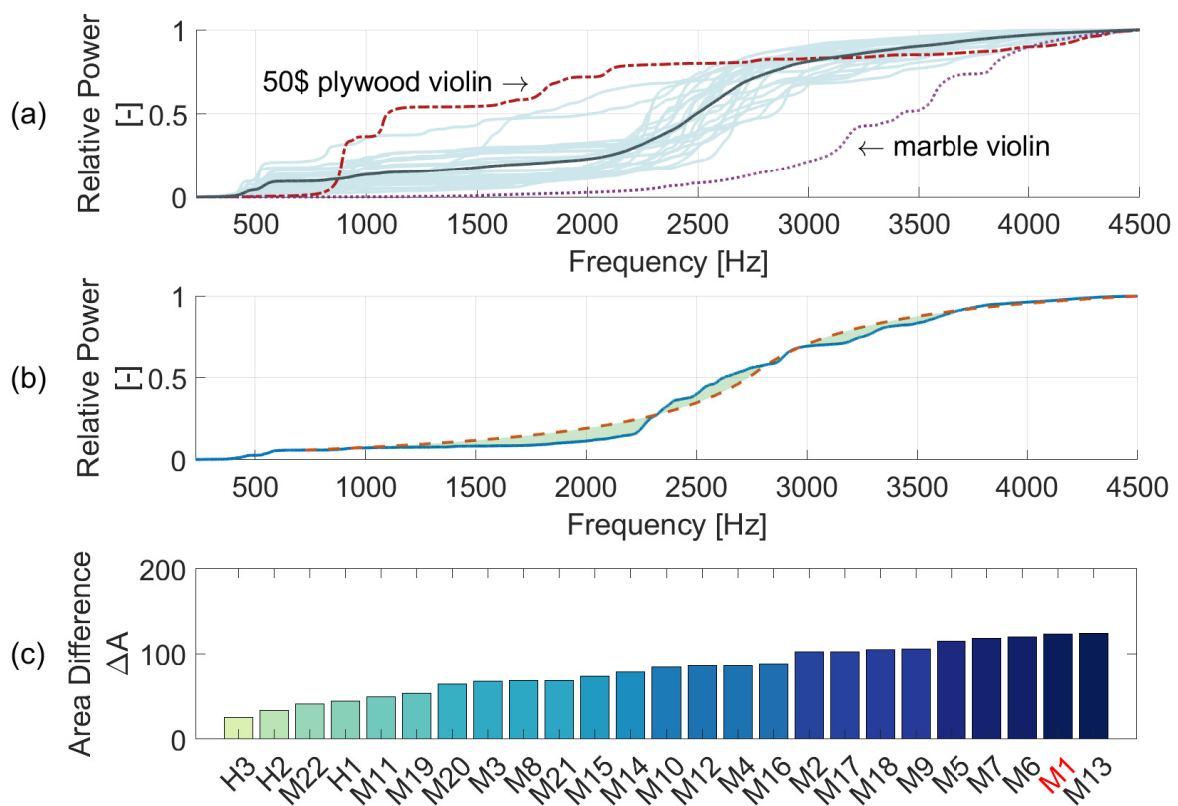


Figure 1. (a) Relative power for all the admittances in the dataset (solid light blue lines). In dashed lines are the same quantity obtained for two “outliers”: a cheap industrial violin made of plywood (dash-dotted dark red line), and a violin made of marble as part of an art project (dotted violet line). The solid dark green line corresponds to the mean over all the RP curves. (b) The relative power of violin M1 (solid blue line) and corresponding sigmoid fit (dashed red line). The accuracy of the fitting is assessed by looking at the area difference (colored in green). (c) Accuracy of the sigmoid fitting in terms of area difference. Violins are sorted for increasing values of ΔA . Anecdotally, the three Stradivari violins and the copy of one of them are the ones with the smallest error while M1 (labeled in red) is one of the worst fits.

2.5. Feature-Based Reconstruction

Given the models for the different components of the bridge admittance in Equations (1) and (6), its magnitude can be reconstructed starting from the corresponding values of low and mid-frequency features as

$$|H_{ij}(\omega)| \sim \left| \sum_{r=1}^4 \frac{\Phi_{ri}\Phi_{rj}}{\omega_r^2 + 2j\omega\xi_r\omega_r - \omega^2} \right| + C \frac{\delta\sigma'(\omega, \omega_{mid}, \omega^*, k^*)}{\delta\omega}, \quad \omega \in [\omega_{min}, \omega_{max}], \quad (7)$$

where C is a constant found through iterative optimization such that the MSE between the second term of Equation (7) and $|H_{ij}(\omega)|$ is minimized around $\omega = \omega^*$.

Figure 2 shows the application of the proposed methodology. Here, one of the historical violins (i.e., H1) is taken as an example. Figure 2a depicts its FRF magnitude. It can be seen that the four signature modes are easily identifiable up to around 700 Hz, while modes are more overlapped for higher frequencies. Using these modes, the reconstruction obtained through modal superposition (Figure 2b) approximates the FRF up to ω_{mid} .

The second component in Equation (7) accounts for the reconstruction of the mid-frequency portion of the FRF (Figure 2c). The parameters controlling $\sigma'(\omega, \omega_{mid}, \omega^*, k^*)$ are the result of the fitting performed on the RP curve of H1.

The combination of the two models in Figure 2d resembles a “cleaner” version of the original measured signal. Indeed, the reconstructed signal keeps the same energy balance between low and mid components. By computing the residual as the relative difference between measure and reconstruction, as depicted in Figure 2e, we can assess where the model fails at recovering the original signal measured.

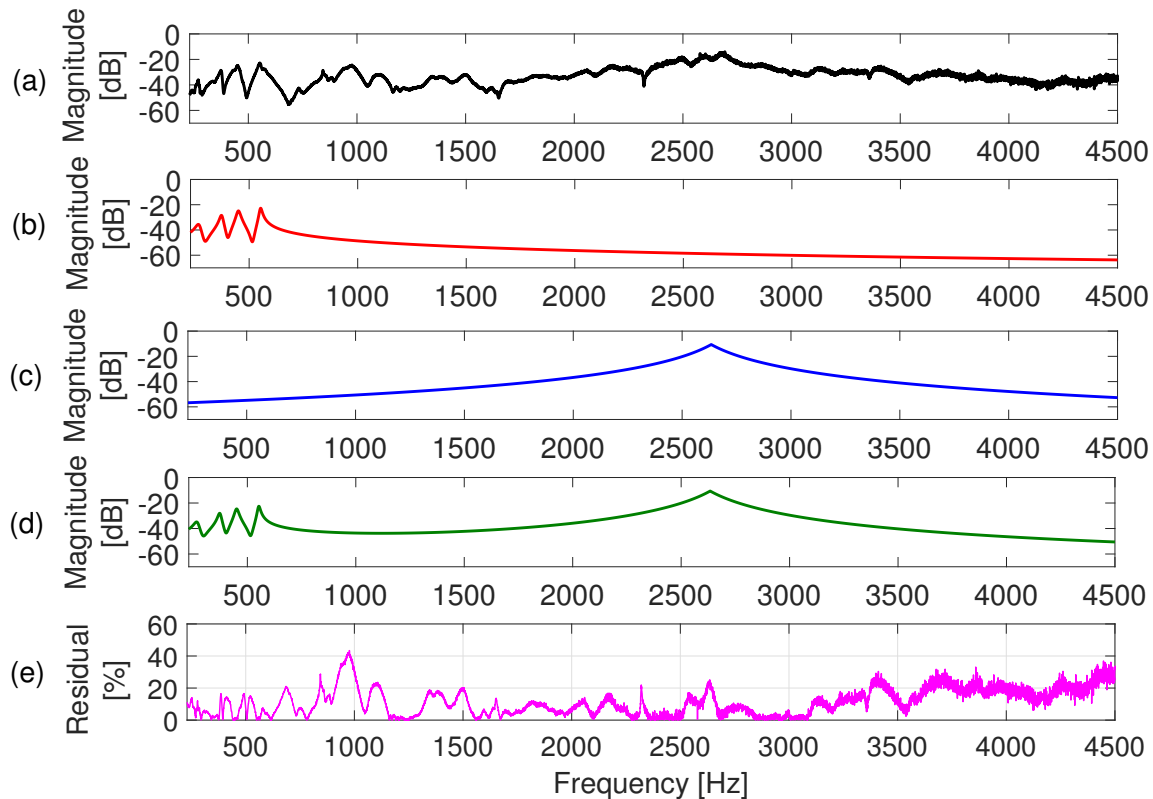


Figure 2. Example of measured bridge admittance and relative feature-based reconstruction. From top to bottom, the original signal (a), its analytical approximation in the low-frequency range through modal superposition (b), its reconstruction based on the sigmoid model in the mid-frequency range (c), and their linear combination (d) are shown. The relative difference between measured and reconstructed signals is assessed in percentage as a function of frequency (e). Magnitudes are reported in [dB re $1 \text{ m s}^{-1} \text{ N}^{-1}$].

In the specific case of H1, the reconstructed signature modes resemble the original ones and the residual oscillates around 5% close to antiresonance frequencies. A relevant increase of the residual up to 40% is then encountered around 1 kHz. The frequency span characterized by large values of the residuals covers the portion of FRF dominated by transitional modes. For a subset of FRFs in the dataset, transitional modes exhibit low mode overlapping and modal superposition may model the FRF better than the proposed energy-based model. However, a common trend was not found throughout the dataset and further research is needed to improve the model within this frequency range.

In the case of H1, the proposed reconstruction is also able to model the region of the FRF between 1500 and 3000 Hz. Here, the residual stabilizes between 5% and 10% except for spikes corresponding to the presence of peaks or deeps in this portion of the spectrum, which cannot be recognized however as individual modes.

Finally, the reconstruction fails at explaining the trend of the admittance for higher frequencies, i.e., between 4000 and 4500 Hz. In this range, the FRF exhibits a more linear trend, and the residual reaches values around 20%. The feature k_{high} has been indeed introduced to overcome this lack of information, defined as the slope of the linear fit limited to the high frequency range mentioned.

3. Results

3.1. Relative Power Analysis

We focus only on the analysis of the estimated RP curves. Indeed, an in-depth discussion of the low-frequency features is already presented in [16].

Figure 1a shows, in terms of relative power, all the violins in the dataset (solid light blue lines) along with two violins that can be considered as “outliers”: on one hand an industrial violin made of plywood (dash-dotted dark red line), and on the other, a violin entirely made of marble, except for the bridge and tailpiece (dotted violet line). It can be noticed that all the RP curves are concentrated in the middle between the two outliers. By computing the mean over all the RP curves in the dataset (dark green solid line), a sigmoidal trend can be observed. Moreover, the largest variation among the RP curves can be observed between 2000 and 3000 Hz if the standard deviation is evaluated as a function of frequency. In this frequency interval, the center of the sigmoid occurs for all the violins in the dataset.

Concerning the clearly different behavior of the outliers, as we said the major difference between them and the other violins is the material used for these instruments. Despite being shifted in the frequency axis, the shape of the RP curves still follows a sigmoidal trend. In the case of plywood, its specific stiffness (i.e., the ratio between the Young’s modulus, being it the constant describing the material stiffness, and the density) is far smaller than typical spruce wood, as well as being less anisotropic [26]. For marble it is the contrary: the material is far stiffer and denser than spruce. Both violins have roughly the same geometric characteristics, in terms of dimensions, arching, and thickness profile, so we can interpret the difference in the RP curves to their vastly different materials. Although a sigmoidal behavior can be seen for the averaged RP, the accuracy of the actual fitting varies from one violin to another. As an example, Figure 1b shows one of the worst sigmoid fits obtained (i.e., violin M1). It can be seen that the sigmoid curve (dashed red line) fails at approximating the measured RP (solid blue line). This may be due to the irregular and bumpy behavior of the RP curve, especially in the frequency range where the sigmoid is centered.

To have a measure of the “regularity” of the energy distribution, we computed the area difference ΔA (Figure 1b, colored in green) throughout the dataset. Figure 1c lists all the resulting values, in ascending order. Anecdotally, the four violins characterized by the lowest values are H3, H2, M22, and H1. These are the three Stradivari violins present in the dataset and a fine modern copy of one of them used by a professional musician. Conversely, the poor fit already observed for M1 corresponds to one of the highest values of ΔA . For the ease of reading, the label of M1 is colored in red in Figure 1c.

From the analysis of the RP curves and the features related, we can conclude that the sigmoid is able to model the majority of the RP curves in the dataset, especially the Stradivari violins.

3.2. Violin Clustering

Given the features defined in Sections 2.3 and 2.4, the resulting feature space considered has thus 19 dimensions, leading to a feature matrix in $\mathbb{R}^{M \times 19}$, where $M = 25$. Z-score normalization [27] has been applied over each feature vector inside the feature matrix to equalize values within a common scale. Once normalized, an Euclidean distance can be computed over the feature vectors characterizing each pair of admittances, leading to a distance matrix $\mathbf{D} \in \mathbb{R}^{M \times M}$. Notice that all the features have the same relative importance to define our distance. In perceptual terms this could not hold, as some features can have a far larger influence than others. However, further studies are needed in this sense to define a “perceptual distance” between instruments.

Figure 3a shows the distance matrix D , with the elements sorted following the hierarchy of a dendrogram [28]. The dendrogram is computed iteratively using farthest neighbor clustering to define the hierarchical relations [29]. In this way, similar violins (i.e., pairs of instruments with a small distance) are clustered together.

We decided to cut the dendrogram at a value of the farthest neighbor distance equal to 50 (vertical cyan line) as the link between H3, M22 and the remaining Stradivari violins occurs at around 48. As a result, four clusters with varying sizes can be observed: (i) M17-M13-M18-M5-M16-M3-M8-M6-M7, (ii) M12-M14-M4-M1-M19-M11-M20-M10-M9, (iii) M21-M15, and (iv) H1-M2-H2-H3.

It is noteworthy that the distance between M22 and H1 is lower than the one assessed between M22 and its model H3. The similarity between M22 and H3 was already confirmed up to 1400 Hz in [16] (referred to as “V1” and “Strad”), where the first ten peaks were chosen as features. To investigate which features the similarity between M22 and H1 mostly relies on, we visually compare the bridge admittance of the three violins.

Figure 3b shows the three FRFs overlapped. Looking at the low-frequency range, the modes of M22 (dash-dotted blue line) resemble both those of its original H3 (dotted red line) and H1 (dashed yellow line). In terms of Euclidean distances, the distance computed considering only the low-frequency features yields comparable values: 7.72 between M22 and H1, and 8.92 between M22 and H3. However, a huge difference can be observed at mid frequencies, where H3 is characterized by a high-energy region centered at a lower frequency (1632 Hz against 2402 Hz for M22 and 2634 Hz for H1) and more limited in amplitude with respect to M22 and H1 (−24.2 dB against −16 dB for M22 and −14.9 dB for H1). Due to this difference, the proposed similarity metric varies greatly between the two pairs of violins: 9.51 between M22 and H1, 17.88 between M22 and H3.

The same considerations can be inferred more clearly by inspecting the corresponding feature-based reconstructions in Figure 3c. In particular, the reconstruction of the high-energy region better highlights its position and width and thus makes the visual comparison between different instruments much easier.

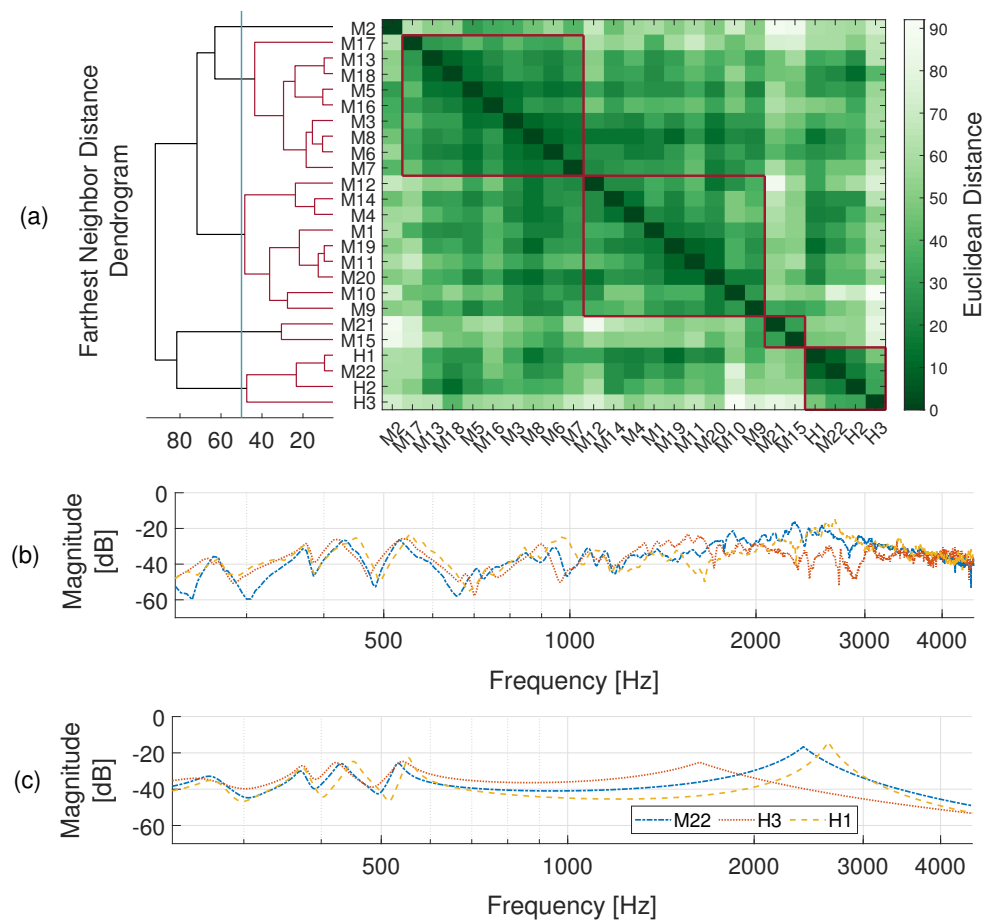


Figure 3. (a) Euclidean distance matrix, with elements sorted following the dendrogram hierarchy. In this way, similar violins cluster together (colored in red). Four clusters are obtained by cutting the dendrogram at a farthest neighbor distance equal to 50 (vertical cyan line). (b) The bridge admittance of M22 (dash-dotted blue line) compared to those of H3 (dotted red line) and H1 (dashed yellow line), and (c) corresponding reconstructions from the feature space. Magnitudes are reported in [dB re $1 \text{ m s}^{-1} \text{ N}^{-1}$]. The similarity between these violins leads to the cluster at the bottom-right corner of the distance matrix. The comparison of the three reconstructions highlights the different similarities: the signature modes of M22 are similar to those of both H3 and H1 while its mid-range resembles more that of H1.

3.3. Correlation between Features and PCA

To understand if these “hand-crafted” features are linearly independent and statistically significant, we computed the Pearson correlation coefficient between the column vectors of the feature matrix extracted from the dataset. Subsequently, we performed principal component analysis on the same matrix.

Figure 4a shows the matrix of the Pearson correlation where the absolute value of the correlation coefficients is reported for each pair of features in the set. The values range between 0 and 1, and moderate or strong correlation occurs for values greater than 0.3 [30].

The signature mode frequencies (f_1, \dots, f_4) generate a cluster inside the matrix, with coefficients ranging between 0.5 and 0.65, therefore they are strongly correlated. Another cluster can be observed for (p_1, \dots, p_4). In this case, the signature mode amplitudes show a moderate correlation with values around 0.3, except for (p_1, p_2) where the largest coefficient occurs in the matrix (0.75). Conversely, an interpretation regarding the correlation coefficients of the signature mode damping (q_1, \dots, q_4) is harder to infer from the matrix. It is interesting to note that indeed the frequency and the amplitude of the peaks seem to be *orthogonal* descriptors of the FRF.

Furthermore, low correlation can be seen in general between the subsets of low-frequency and mid-frequency features. By looking at the submatrix on the bottom-left of Figure 4a (outlined by dashed red lines), the only correlated features are ω_{mid} , RP_{mid} and ω^* . Indeed, ω_{mid} and ω^* are linearly related to (f_1, \dots, f_4) while RP_{mid} is strongly correlated with (p_3, p_4) .

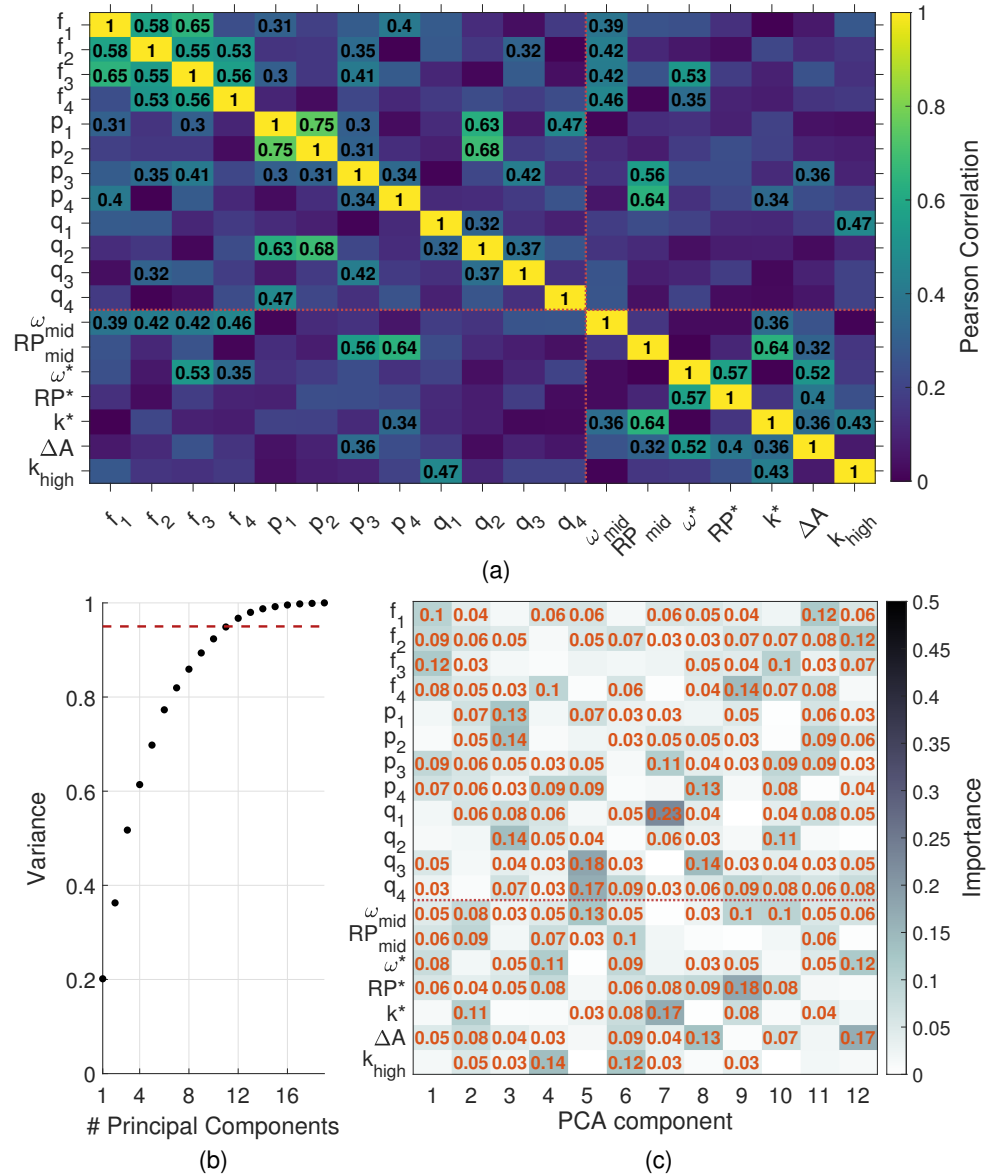


Figure 4. (a) Matrix of the Pearson correlation between features. The absolute value of the coefficients, ranging between 0 and 1, is reported. Explicit values are shown only for combinations of features with moderate and strong correlation (≥ 0.3). (b) The normalized cumulative sum of the eigenvalues obtained with PCA. A dashed red line highlights how many components are needed to recover 96.7% of the original information. (c) Feature importance in the first twelve principal components. Explicit values are shown only when greater than 0.05. Interestingly enough, frequencies and amplitudes in signature modes are almost independent and the mid-frequency features mainly constitute the second principal component.

If we limit the analysis to the subset of mid-frequency features, the sigmoid curvature k^* and the area difference ΔA show a correlation coefficient above 0.3 with most of the other features. On one hand, the curvature of the RP curve (k^*) is correlated to its behavior at the extremes of the range: strong correlation with RP_{mid} (0.64) and moderate correlation

with k_{high} (0.43), ω_{mid} (0.36), and ΔA (0.36). On the other hand, strong correlation can be observed between ΔA and features characterizing the central part of the sigmoid: ω^* (0.52), RP^* (0.4), k^* (0.36), and RP_{mid} (0.32). As a consequence, one could infer an estimate for k^* starting from $(\omega_{mid}, RP_{mid}, k_{high}, \Delta A)$ and for ΔA given $(\omega^*, RP^*, k^*, RP_{mid})$.

Figure 4b shows the cumulative sum of the eigenvalues obtained with PCA. The cumulative function is normalized such that the eigenvalues sum to 1. Twelve principal components out of nineteen account for 96.7% of the total variance of the set.

Figure 4c shows the absolute value of the coefficients for the first twelve principal components. We normalized the resulting values such that the sum is equal to 1 for each component.

Although no clear patterns can be observed inside the matrix, it can be noticed that some features contribute more than others. Indeed, frequencies (f_1, \dots, f_4) dominate the first principal component, with values greater than 0.08. Additionally, the amplitudes (p_1, \dots, p_4) show noticeable values in the most informative components (1 and 3). Conversely, the damping features (q_1, \dots, q_4) start occurring later inside the PCA vectors (only after the third). Interestingly enough, the mid-frequency features occur in the first two principal components. We can thus conclude that the mid-frequency features are as statistically significant as modal frequencies and amplitudes in defining an FRF. To the best of our knowledge this is the first result showing such objective relevance of the mid range features.

4. Discussion

The features we have defined to compare violins have three advantages with respect to the literature: (a) they are objectively defined and they can be easily computed from any FRF. (b) They can be used to roughly reconstruct the FRF signal with just a handful of parameters. This could be extremely useful in virtual analog simulations of instruments [13], as an example. (c) They provide a reduced dimensional representation of the FRF whence an objective distance metric can be computed. Hitherto in the literature, this comparison has been purely visual and subjective.

One of these features, i.e., the degree to which the high power spectrum approximates a sigmoid function, has been found to anecdotally correlate with the subjective quality of the instruments: three Stradivari and one bench copy of one of them have the lowest values for this feature. The copy of the Stradivari is in possession of a renowned professional musician, and he states that both violins have a very similar sound.

We have also found that these quality violins live in a “Goldilocks zone” for relative power. That Goldilocks zone seems to depend on the material of the instrument: if the material is too soft, the instrument has no tone, as the cheap violin shows. If the material is too stiff, as in the case of the marble violin, there is no body to the sound and it lacks projection. Studying in depth how design and material parameters influence the shape of the relative power may give valuable insights in how to craft a quality instrument.

Once the bridge admittances are projected into the feature representation, one can assess the similarity between different instruments by simply computing a Euclidean distance. Additionally, in this case, the three Stradivari and the modern copy have been found to cluster together.

If compared to the feature representation presented in [16], the extension of the representation to the mid-frequency range led to a more informative similarity metric. Indeed, the new Euclidean distance highlighted that the bench copy is more similar to another Stradivari violin rather than its original. By comparing the reconstructed FRFs, it is clear that the difference relies on the frame of the signal related to the so-called bridge hill.

This evidence, together with the importance of the mid-frequency features highlighted by PCA, may suggest that not only the shape and the material used for the violin soundbox but also its interaction with the other components (i.e., the bridge) play a crucial role in defining the characteristics of the instrument. Studying the impact of the violin setup (e.g., tuning of the bridge and the tailpiece) on these features may give a new tool to violin makers and musicians to design the violin sound from a vibrational standpoint.

One limitation is that our model does not consider the transitional modes between 700 and 1200 Hz, but they could be easily included. Our own research does show, however, that at least for the top plate [10], the higher modes are highly correlated with the low modes so its inclusion should not change the clustering or the definition of the distance matrix. To overcome this limitation, a possible extension of the current feature set could be envisioned through the definition of additional descriptors derived from the RP curve. These new features could deal with transitional modes separately from the mid-frequency range, as a simpler alternative to mode fitting.

In its current version, the feature representation proposed allows the comparison between different instruments only in terms of vibration. Indeed, how much these features are relevant from a perceptual point of view and how they should be “prioritized” while designing a musical instrument are still open questions. However, the proposed methodology could be used to synthesize a variety of “virtual” violins to assess the perceptual weights of the features through listening tests [31]. Since most of the features presented here seem to be possible to predict from the material and geometric parameters of the instrument [32], the dream of having a virtual workbench where one can sonically design an instrument to optimize perception is one step closer.

Author Contributions: R.M. performed the vibration tests; R.M., S.G. and F.A. designed the feature representation and analyzed the data; R.M. and S.G. wrote the paper; A.S. and R.C. supervised the work. All authors have revised the manuscript. All authors have read and agreed to the published version of the manuscript.

Funding: This research received no external funding.

Institutional Review Board Statement: Not applicable.

Informed Consent Statement: Not applicable.

Data Availability Statement: The data presented in this study are available on request from the corresponding author. The data are not publicly available due to privacy restrictions.

Acknowledgments: The authors would like to thank the “Fondazione Stradivari—Museo del Violino” and the curator of the museum M° F. Cacciatori for offering some of the instruments of the collection and all the participants who joined the measurement campaign during Mondo Musica 2020.

Conflicts of Interest: The authors declare no conflict of interest.

Abbreviations

The following abbreviations are used in this manuscript:

FRF	Frequency Response Function
MSE	Mean Square Error
RP	Relative Power
PCA	Principal Component Analysis

References

1. Fritz, C.; Curtin, J.; Poitevineau, J.; Tao, F.C. Listener evaluations of new and Old Italian violins. *Proc. Natl. Acad. Sci. USA* **2017**, *114*, 5395–5400. [[CrossRef](#)] [[PubMed](#)]
2. Fritz, C.; Curtin, J.; Poitevineau, J.; Morrel-Samuels, P.; Tao, F.C. Player preferences among new and old violins. *Proc. Natl. Acad. Sci. USA* **2012**, *109*, 760–763. [[CrossRef](#)]
3. Rozzi, C.A.; Voltini, A.; Antonacci, F.; Nucci, M.; Grassi, M. A listening experiment comparing the timbre of two Stradivari with other violins. *J. Acoust. Soc. Am.* **2022**, *151*, 443–450. [[CrossRef](#)] [[PubMed](#)]
4. Rau, M.; Abel, J.S.; Smith, J.O., III. Contact sensor processing for acoustic instrument recording using a modal architecture. In Proceedings of the International Conference of Digital Audio Effects, Aveiro, Portugal, 4–8 September 2018.
5. Gough, C. Acoustic characterisation of string instruments by internal cavity measurements. *J. Acoust. Soc. Am.* **2021**, *150*, 1922–1933. [[CrossRef](#)] [[PubMed](#)]
6. Woodhouse, J. On the “bridge hill” of the violin. *Acta Acust. United Acust.* **2005**, *91*, 155–165.
7. Durup, F.; Jansson, E.V. The quest of the violin bridge-hill. *Acta Acust. United Acust.* **2005**, *91*, 206–213.
8. Woodhouse, J. Body vibration of the violin—What can a maker expect to control. *Catgut Acoust. Soc. J.* **2002**, *4*, 43–49.

9. Woodhouse, J. The acoustics of the violin: A review. *Rep. Prog. Phys.* **2014**, *77*, 115901. [CrossRef]
10. Gonzalez, S.; Salvi, D.; Baeza, D.; Antonacci, F.; Sarti, A. A data-driven approach to violin making. *Sci. Rep.* **2021**, *11*, 1–9.
11. Bissinger, G. The violin bridge as filter. *J. Acoust. Soc. Am.* **2006**, *120*, 482–491. [CrossRef]
12. Rau, M. Measurements and analysis of acoustic guitars during various stages of their construction. *J. Acoust. Soc. Am.* **2021**, *149*, A25–A25. [CrossRef]
13. Rau, M.; Abel, J.S.; James, D.; Smith III, J.O. Electric-to-acoustic pickup processing for string instruments: An experimental study of the guitar with a hexaphonic pickup. *J. Acoust. Soc. Am.* **2021**, *150*, 385–397. [CrossRef] [PubMed]
14. Maestre Gómez, E.; Scavone, G.P.; Smith, J.O. Digital modeling of bridge driving-point admittance from measurements on violin-family instruments. In Proceedings of the Stockholm Music Acoustics Conference 2013, Stockholm, Sweden, 30 July–3 August 2013; Bresin, R., Askenfelt, A., Eds.; Logos Verlag: Berlin, Germany, 2013; pp. 101–108.
15. Woodhouse, J.; Langley, R. Interpreting the Input Admittance of Violins and Guitars. *Acta Acust. United Acust.* **2012**, *98*, 611–628. [CrossRef]
16. Malvermi, R.; Gonzalez, S.; Quintavalla, M.; Antonacci, F.; Sarti, A.; Torres, J.A.; Corradi, R. Feature-based representation for violin bridge admittances. In Proceedings of the “Advances in Acoustics, Noise and Vibration—2021” the 27th International Congress on Sound and Vibration, Online, 11–16 July 2021.
17. The Permanent Collection of Contemporary Violinmaking. Available online: <https://www.museodelviolino.org/en/museo/percorso-museale/sala-8-il-concorso-triennale-di-liuteria-contemporanea/> (accessed on 12 May 2022).
18. Vasques, C.; Rodrigues, J.D. *Vibration and Structural Acoustics Analysis: Current Research and Related Technologies*; Springer Science & Business Media: Berlin/Heidelberg, Germany, 2011.
19. Kiesel, T.; Langer, P.; Marburg, S. Numerical Study on the Effect of Gravity on Modal Analysis of Thin-Walled Structures. *Acta Acust. United Acust.* **2019**, *105*, 545–554. [CrossRef]
20. Schwarz, B.J.; Richardson, M.H. Experimental modal analysis. *CSI Reliab. Week* **1999**, *35*, 1–12.
21. Gough, C.E. A violin shell model: Vibrational modes and acoustics. *J. Acoust. Soc. Am.* **2015**, *137*, 1210–1225. [CrossRef]
22. Meirovitch, L. *Fundamentals of Vibrations*; McGraw-Hill Higher Education, McGraw-Hill: New York, NY, USA, 2001.
23. Curtin, J. Scent of a violin. *STRAD* **2009**, *120*, 30–33.
24. Chopra, A.K. *Dynamics of Structures: Theory and Applications to Earthquake Engineering*; Pearson: London, UK, 2006.
25. Normalized Tunable Sigmoid Function. Available online: <https://dhemery.github.io/DHE-Modules/technical/sigmoid/> (accessed on 22 May 2022).
26. Ross, R.J. Wood handbook: Wood as an engineering material. In *USDA Forest Service, Forest Products Laboratory, General Technical Report FPL-GTR-190, 2010: 509 p. 1 v*; U.S. Department of Agriculture, Forest Service, Forest Products Laboratory: Madison, WI, USA, 2010; Volume 190. [CrossRef]
27. Jain, A.; Nandakumar, K.; Ross, A. Score normalization in multimodal biometric system. *Pattern Recognit.* **2005**, *38*, 2270–2285. [CrossRef]
28. Gruvaeus, G.; Wainer, H. Two additions to hierarchical cluster analysis. *Br. J. Math. Stat. Psychol.* **1972**, *25*, 200–206. [CrossRef]
29. Defays, D. An efficient algorithm for a complete link method. *Comput. J.* **1977**, *20*, 364–366. [CrossRef]
30. Cohen, J. *Statistical Power Analysis for the Behavioral Sciences*; Routledge: London, UK, 2013.
31. Fritz, C.; Cross, I.; Moore, B.C.; Woodhouse, J. Perceptual thresholds for detecting modifications applied to the acoustical properties of a violin. *J. Acoust. Soc. Am.* **2007**, *122*, 3640–3650. [CrossRef] [PubMed]
32. Badiane, D.G.; Malvermi, R.; Gonzalez, S.; Antonacci, F.; Sarti, A. On the Prediction of the Frequency Response of a Wooden Plate from Its Mechanical Parameters. In Proceedings of the ICASSP 2022–2022 IEEE International Conference on Acoustics, Speech and Signal Processing (ICASSP), Singapore, 22–27 May 2022; pp. 461–465. [CrossRef]